THESIS FOR THE DEGREE OF DOCTOR OF PHILOSOPHY IN SOLID AND STRUCTURAL MECHANICS

Modeling and experimental characterization of large biaxial strains and induced anisotropy in pearlitic rail steel

KNUT ANDREAS MEYER

Department of Industrial and Materials Science
Division of Material and Computational Mechanics
CHALMERS UNIVERSITY OF TECHNOLOGY

Gothenburg, Sweden 2019

Modeling and experimental characterization of large biaxial strains and induced anisotropy in pearlitic rail steel
KNUT ANDREAS MEYER
ISBN 978-91-7905-155-6

Doktorsavhandlingar vid Chalmers tekniska högskola
Ny serie nr. 4622
ISSN 0346-718X
Department of Industrial and Materials Science
Division of Material and Computational Mechanics
Chalmers University of Technology
SE-412 96 Gothenburg
Sweden
Telephone: +46 (0)31-772 1000

Cover:
Undeformed test bar (left), simulated residual shear stress in a cross-section of the bar (center) and deformed test bar (right).

Chalmers Reproservice
Gothenburg, Sweden 2019

Modeling and experimental characterization of large biaxial strains and induced anisotropy in pearlitic rail steel
Thesis for the degree of Doctor of Philosophy in Solid and Structural Mechanics
KNUT ANDREAS MEYER
Department of Industrial and Materials Science
Division of Material and Computational Mechanics
Chalmers University of Technology

Abstract

Large shear strains accumulate in the near-surface region under the running band of railway rails. In this region, rolling contact fatigue cracks often initiate, causing major problems for the railway industry. However, characterization of the constitutive and fatigue behavior of the material in this region is difficult due to the high strain gradient. The solution proposed in this thesis is to produce highly deformed cylindrical test bars: An axial-torsion test rig is used to predeform the bars in torsion while subjected to axial compressive loading. The obtained material state is found to be similar to that of field samples of rails at a depth between 50 and 100 µm. Using this predeformation method, the evolution of the yielding behavior is evaluated. The predeformed test bars are re-turned and drilled out to form thin-walled test bars, which can be used to measure yield surfaces. It is found that the degree of anisotropy quickly evolves with increasing predeformation and then saturates. Furthermore, the quadratic Hill yield criterion describes the anisotropic yield surfaces well.

To better optimize rail maintenance and material selection, there is an industrial need for a model capable of predicting rail deterioration. An important component of such a model is an accurate material model that captures the relevant physical phenomena. A hyperelasto-plastic framework for finite strain material models is adopted in this thesis. As a first study, the predeformation method was simulated using 2D axisymmetric elements. It is shown that very good results can be achieved by using material models with advanced kinematic hardening laws. Next, an improved simulation methodology for axial, torsional and pressure loading is developed, resulting in an efficient 1D formulation. This methodology includes material removal to simulate the re-machining of the test bars into tubular bars. Using this methodology, 3 different distortional hardening models are evaluated in terms of how well they fit and predict the experimental data. The two phenomenological models perform better than the crystal plasticity model. However, these models should be further developed to improve their predictive abilities.

Keywords: Pearlitic steel, hyperelasto-plasticity, biaxial loading, axial-torsion, kinematic hardening, yield criteria, distortional hardening

Til mine største forbilder og støttespillere:
Mamma og Pappa

Preface

The work in this thesis was carried out at the Department of Industrial and Materials Science at Chalmers University of Technology from May 2015 to August 2019 within the research project MU34 "Influence of anisotropy on the deterioration of rail materials". This project has been part of the research activities in the National Centre of Excellence CHAlmers Railway MEChanics (CHARMEC). The research has been funded by Chalmers, Trafikverket (via the European Horizon 2020 Joint Technology Initiative; Shift2Rail through contract no. 730841 and In2Track2 under grant agreement no. 826255), voestalpine Schienen GmbH and the other industrial partners to CHARMEC.

The experimental work in this thesis is based on the axial-torsion testing machine, acquired by CHARMEC in late 2015. Professor Johan Ahlström had the idea of the predeformation technique developed in this thesis: The goal was to be able to test the rail and wheel materials under realistic multiaxial loading conditions.

Acknowledgements

I would like to start by thanking my science teachers in chronological order. In Norway, Harald Ruud for letting me explore the sciences (and almost blow up the chemistry lab) and Ivar Helgesen †, Arnt Frode Stava and Anne-Elisabeth Indrebø Haga for challenging me and still trusting me after "warnings" from Harald. At Chalmers, Professor Mikael Enelund and the team around him have created an impressive mechanical engineering program: I am particularly grateful for the support to the student society "eXPerimentverkstaden", through which I gained a lot of workshop experience. Much of the experimental work in this thesis would not have been possible without this experience. Last of my teachers, but certainly not the least, my supervisors: Professor Magnus Ekh and Professor Johan Ahlström are greatly appreciated for their guidance, encouragement and care throughout these past years. The amount of knowledge you possess is only matched by your abilities to share it. I feel very lucky to have been supervised by you two, getting the best of two worlds: Computational mechanics and materials science.

Furthermore, I would like to thank my other co-author Dimitrios Nikas for a very interesting and fun cooperation. Håkan Millqvist has been very welcoming and helpful in the materials workshop, for which I am very grateful. My dear friends and colleagues at the divisions of "Material and Computational Mechanics", "Dynamics" and "Engineering Materials" are also much appreciated, and I really appreciate all of our interesting discussions about research, life and anything in-between.

Finally, I would like to thank my family and friends for always being there for me. Especially, I want to thank my parents for the many good values in life and their unconditional love and support: I would not be the man I am today without you.

Thesis

This thesis consists of an extended summary and the following appended papers:

Paper A Meyer, K.A., Nikas, D., Ahlström, J. "Microstructure and mechanical properties of the running band in a pearlitic rail steel: Comparison between biaxially deformed steel and field samples" *Wear* vol. 396–397, pp. 12–21 (2018)

Paper B Meyer, K.A., Ekh, M. "A comparison of two frameworks for kinematic hardening in hyperelasto-plasticity" *XIV International Conference on Computational Plasticity (COMPLAS 2017)* (2017)

Paper C Meyer, K.A., Ekh, M., Ahlström, J. "Modeling of kinematic hardening at large biaxial deformations in pearlitic rail steel" *International Journal of Solids and Structures* vol. 130–131, pp. 122–132 (2018)

Paper D Meyer, K.A., Ekh, M., Ahlström, J. "Anisotropic yield surfaces after large shear deformations in pearlitic steel" *Submitted for international publication* (2019)

Paper E Meyer, K.A., Ekh, M., Ahlström, J. "Material model calibration against axial-torsion-pressure experiments accounting for the non-uniform stress distribution" *Finite Elements in Analysis and Design* vol. 163, pp. 1-13, (2019)

Paper F Meyer, K.A. "Evaluation of material models describing the evolution of plastic anisotropy in pearlitic steel" *Submitted for international publication* (2019)

The appended papers were prepared in collaboration with the co-authors. **Paper A** was a joint work between CHARMEC projects MU28 (Dimitrios Nikas) and MU34, in which the experimental work was shared. In **Paper B** - **Paper E** the author of this thesis was responsible for the major progress of the work, i.e. planning and writing the papers, took part in developing the theory, planning and conducting the experiments, developing the numerical implementations and running the simulations.

Part III contains a correction of Figure 8 in **Paper A** that was discovered after publishing.

Contents

Part I
Extended Summary

1 Introduction

A major advantage of railway transportation is the low rolling resistance in the wheel-rail contact. Unfortunately, this comes at the cost of very high contact pressure, which can exceed 1000 MPa (Johnson 1989; Pau et al. 2002; Marshall et al. 2006; Wiest et al. 2008). The small contact patch also results in high shear stresses due to traction and cornering forces, resulting in wear and severe plastic deformations. These processes lead to large geometric changes of the railhead during service, which are visualized in Figure 1.1a using a field sample from **Paper A**. The severe plastic deformations close to the surface are visible in the material after etching; see Figure 1.1b

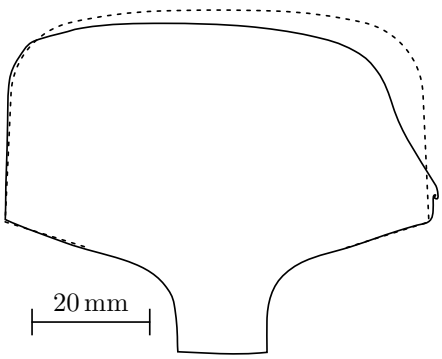

(a) *Nominal rail profile (BV50) (dashed line) and a worn and deformed profile (solid line) from **Paper A**.*

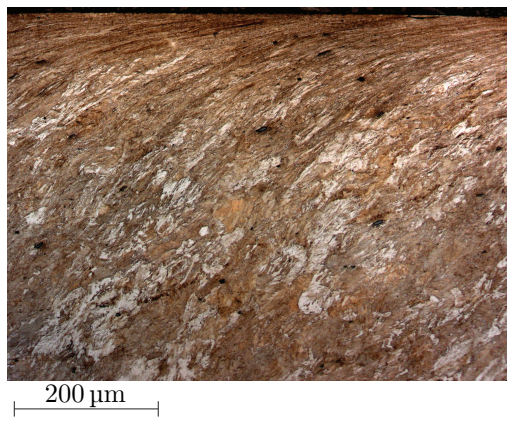

(b) *Flow lines showing the highly deformed material at the gauge corner of the rail (45° to the longitudinal direction.*

Figure 1.1: *Visualization of the large deformations in a rail from the Swedish main line between Gothenburg and Stockholm.*

In 2012, the annual cost for railway infrastructure maintenance and renewal across Europe was estimated to be between 15 and 25 billion Euros (EIM-EFRTC-CER WORKING GROUP 2012). The cost of rail defects alone in the '90s was estimated at 2 billion Euros a year by Cannon et al. (2003). This equates to an average cost of about 6700 Euro per kilometer in Europe's 300 000 km long railway network (Lidén and Joborn 2016). These costs do not include the lost profit due to scheduled maintenance, nor the loss of profit for business passengers during delays due to unscheduled repairs.

For the railway industry it is important to be able to predict the deterioration due to the wheel-rail interaction. An overall goal for much of the research within CHARMEC is

to develop the necessary components for a model with such predictive capability. Some of these components are

- Dynamic simulations of the interaction between train and track.
- Finite Element (FE) modeling of rail-wheel contact.
- Wear modeling.
- Constitutive modeling of the rail and wheel materials.
- Rolling Contact Fatigue (RCF) initiation criteria.
- Modeling of crack propagation.

Such a model can be used to improve the maintenance efficiency, optimize the material choice and determine requirements for material development. The three last components listed above require detailed knowledge about the mechanical behavior of the rail and wheel material. In particular the behavior of the material in the surface layer is important as RCF is known to initiate there (see Johnson 1989, for an overview). But the high strain gradient, as observed in Figure 1.1b, makes it difficult to test the mechanical behavior of the material. Methods for characterizing the material in this region are therefore needed to obtain experimental data for material model development.

The experimental work in this thesis is relevant for the evaluation of constitutive behavior, fatigue initiation and crack propagation in the surface layer of rails and wheels. However, a majority of the present work deals with the modeling of the constitutive behavior of the material. There has been much focus on modeling the large deformations occurring in railway applications within CHARMEC. In particular, the projects MU14 (Johansson 2006) and MU19 (Larijani et al. 2014) have addressed the modeling of large plastic deformations. This thesis is a result of the CHARMEC project MU34: "Influence of anisotropy on deterioration of rail materials". The goal of this project is to build upon the previous efforts in MU14 and MU19, with the goal of closing the gap between the modeling and the experimental quantification of rail material behavior during large deformations.

1.1 Aims of thesis

The specific aims of this thesis can be summarized as follows:

1. **Obtain test bars with similar properties as the surface layer of rails**

   A very high strain gradient is present in the surface layer of rails, see Figure 1.1b. This makes it very difficult to do bulk testing of the material. An equivalent material with a uniform strain would greatly simplify the material characterization.

2. **Determine how the behavior of the material in the surface layer of rails evolves**

   RCF is known to initiate in the heavily deformed surface layer of railway rails. But due to the complications described above, little is known about the behavior of

the material in this region. It is therefore interesting to study how the mechanical behavior changes with an increasing amount of deformation.

3. **Model the behavior of the material in the surface layer of rails.**

   To predict RCF initiation and crack propagation, accurate predictions of stresses and strains are required. Material models, which can capture the changing behavior during the service life of a rail, are therefore an important component in a predictive model for deterioration of wheels and rails.

1.2 Limitations

To limit the scope of the thesis, the research is subjected to the following limitations:

- **Only the pearlitic rail steel grade R260 is investigated.**

  By only considering one material grade, more extensive and complex experiments can be conducted. Hence, better data for evaluation of material models for that grade can be obtained. The disadvantage of only using one material is that less general conclusions regarding the applicability of the experimental procedures and the models can be drawn.

- **Multiscale modeling is not considered**

  Multiscale models have great potential for predicting material behavior in terms of the microstructural parameters. However, for use in large-scale simulations of the wheel-rail interaction, such models are still too computationally expensive. They are therefore not considered in this thesis.

- **Modeling of damage and fatigue is not considered**

  Modeling of damage, fatigue and crack propagation in the heavily deformed rail material are very important for predicting the deterioration. Much work has already been conducted within other CHARMEC projects, as well as in other studies reported in the literature. Each of those topics requires extensive research on their own and are not treated in this thesis.

2 The R260 steel grade

The material studied in this thesis is the railway steel grade R260 with a chemical composition according to Table 2.1. It is typically used on the straight track segments with relatively low axle loads (Pointner et al. 2006).

The microstructure is almost fully pearlitic. Pearlite consists of hard cementite lamellas embedded in a ferrite matrix (See Figure 2.1). It is typically arranged in so-called pearlite colonies, in which the cementite lamellas are relatively aligned compared to those in the neighboring colonies. The strength of the pearlitic steel is often attributed to the cementite lamellas acting as obstacles for dislocation motion, cf. Izotov et al. (2007). With increasing plastic deformations the lamella spacing decreases and a large increase in strength can be observed (see e.g. Li et al. 2012; Pippan and Hohenwarter 2016). Bent lamellas were observed after large shear deformations, see Figure 2.1b. Zhang et al. (2018) even observed broken lamellas. At even larger strains, several authors have reported that the cementite dissolves into the ferrite. However, the extent of this dissolution is debatable according to Gavriljuk (2002).

Table 2.1: Composition (in mass percentage) of elements in the R260 steel (in addition to iron), analyzed according to ASTM E 572, 1086 and 1029

C	Si	Mn	P	S	Cr	Al	V	N	Cu
0.72	0.31	1.04	0.006	0.01	0.02	<0.002	<0.005	0.006	0.018

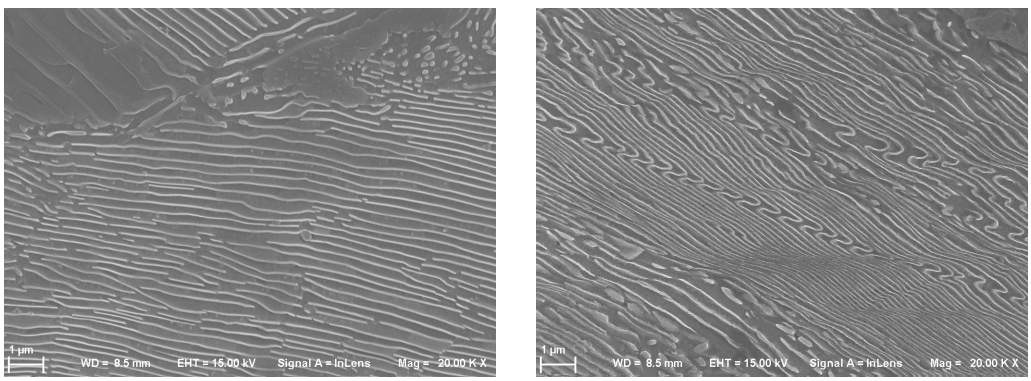

(a) *The undeformed material state* (b) *The deformed material state*

Figure 2.1: *Scanning electron microscope image of the pearlitic microstructure consisting of cementite lamellas (bright contrast) embedded in the ferrite matrix (dark gray contrast)*

3 Predeformation

As discussed in Subsection 1.1, due to the high strain gradients in the surface layer of field samples of rails, testing of the behavior of the material from this region is difficult. Alwahdi et al. (2013) investigated the strain and hardness gradient in such samples. While it could be possible to extract thin strips from the rails and test their mechanical properties, the author of this thesis is not aware of any such studies. The limited size of such specimens would make multiaxial testing challenging. Furthermore, the large scatter in the material structure in field samples would make it difficult to draw conclusions about anisotropic properties. Due to these limitations with direct testing, several studies have been conducted on materials subjected to large shear strains. To obtain a severely deformed pearlitic steel Wetscher et al. (2007) used Equal Channel Angular Pressing (ECAP) while Hohenwarter et al. (2011) and Kammerhofer et al. (2013) used High Pressure Torsion (HPT). These studies primarily deals with changes in the fracture and crack propagation behavior. A main limitation of the ECAP and HPT methods is the small size of the test samples that can be extracted for further characterization. The main advantage with these methods is that very large shear strains can be obtained, in particular for the HPT method.

Many researchers have investigated how pearlitic steel responds to large deformations in general. The most common deformation method is wire drawing. Very high strength materials can be obtained with this method: Li et al. (2012) achieved a yield limit of 6.3 GPa in a hypereutectoid steel. Due to the small diameters of the heavily drawn wires, multiaxial testing is again difficult for this material. Zhao et al. (2014) did perform torsion tests on 1.26 mm drawn wires, but the actual stress-strain behavior could only be approximated as solid samples were used. Another interesting option is sheet metal rolling of pearlitic steels. Very high strengthening was found by Tagashira et al. (2000), but the strength of these steels makes the rolling process challenging.

In **Paper C** a new method for predeformation is proposed, consisting of twisting solid cylindrical test bars under high axial loads. The details of this method are outlined in Subsection 3.1 below. In **Paper A** it was investigated if the predeformation method could be used to achieve a material with similar properties to that of the surface layer of rails. The findings from **Paper A** are described in Subsection 3.2.

3.1 Experimental setup

A wheel rolling over the rail with traction subjects the surface layer of the rail to shear loading combined with high compressive stresses. To achieve the same large shear strains as in the surface layer of rails, axial loading is combined with twisting of test bars in an axial-torsion testing machine. A flow chart describing the loading sequence of the predeformation method is given in Figure 3.1a. The maximum rotation for the used axial-torsion testing machine is 90°. With this limit, the loading becomes a low cycle loading consisting of very large strain increments in each cycle. One advantage of using multiple steps is that both kinematic and isotropic hardening can be identified, provided that yielding occurs upon unloading.

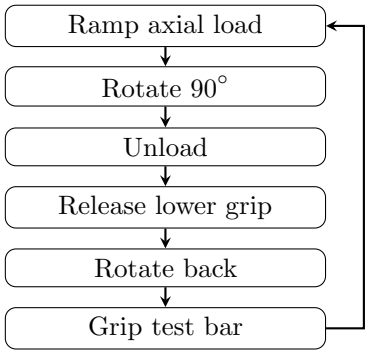

(a) *Flow chart of the predeformation method*

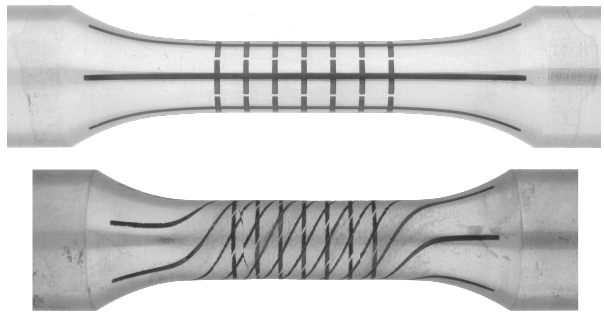

(b) *Undeformed (top) and deformed (bottom) test bar.*

Figure 3.1: *Experimental setup of predeformation*

In Figure 3.1b the surface shear strain is visualized by laser-etched lines for a test bar subjected to 500 MPa nominal compressive load. The undeformed and deformed test bars are shown with the same scale, and the shortening of the test bar due to the compressive loading is visible. The bar diameter also increases in the gauge section due to volume conservation during plastic flow. The shortening during the compressive loading is also shown on the axial mechanical response in Figure 3.2a. Another feature of the experiments, which is also seen in Figure 3.2, is the increase of twist before failure when the amount of compressive axial load is increased. The magnitude of this load was limited

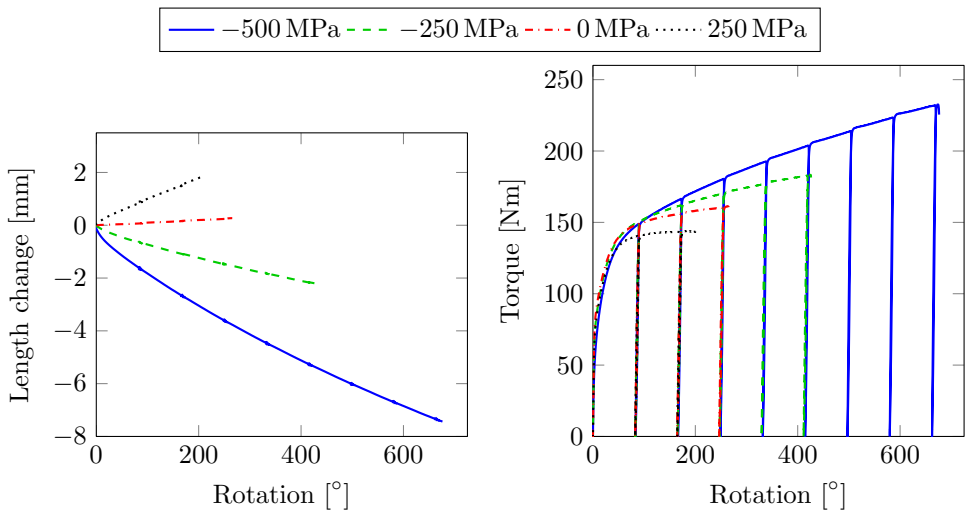

(a) *Change of test bar length.*

(b) *Torque response.*

Figure 3.2: *Test results at different nominal axial stresses.*

due to buckling of the test bars. For the 10 mm diameter test bars, used in **Paper A** and **Paper C**, 600 MPa was the highest successfully applied compressive nominal stress. This stress was also used in **Paper D** and onwards when test bars with 14 mm diameter were used. Higher axial stress could probably have been used to obtain larger shear strains, but 600 MPa gives an axial force close to the maximum limit of the testing machine.

A mechanical extensometer was used to measure the surface strains in the gauge section in **Paper A** and **Paper C**. This could, however, only measure relatively small strains and had to be removed early in the first load cycle. In these papers, the displacement and rotation of the entire test bar were therefore used to evaluate the deformations, as in Figure 3.2. A method using stereo Digital Image Correlation (DIC) to obtain the average surface strains in the gauge section was developed in **Paper E**. By using a moving reference state, the full strain history could be measured. This improvement of the strain measurement significantly simplifies the simulation described in Section 6.

3.2 Verification of method

As previously mentioned, the purpose of the predeformation method is to obtain a microstructure similar to that found in the surface layer of in-service railway rails. The microstructures in the surface layer of field samples were compared to that of the predeformed material in **Paper A**. Three different measures were used to compare the samples:

- Microhardness
- Accumulated shear strains (shear lines)
- Cementite reorientation

The main findings in this paper are that the predeformation technique results in a consistent microstructure and properties that fall within the scatter of field samples. Hence, this method can be used to evaluate the properties of the surface layer of rails. Figure 3.3 shows the shear strain $\tilde{\gamma}$ as a function of depth in the rail samples. The shear in the predeformed test bars is also included, showing the consistency in the amount of shear strain. $\tilde{\gamma}$ is a measure of the shear strain that is based on the evaluation of the optically visible flow lines in e.g. Figure 1.1b. Further characterization of the predeformed material using Transmission Electron Microscope (TEM) was conducted in Nikas et al. (2018). In this study, the evolution of the dislocation density was compared with the hardness and the accumulated shear strain. No comparisons with field samples were made.

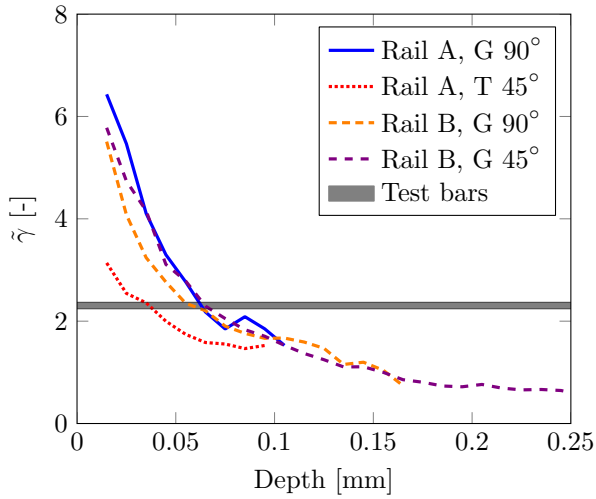

Figure 3.3: *Shear measure $\tilde{\gamma}$, excluding the first* 10 µm

4 Evolution of yield surfaces

A lot of the previous research on the properties of the material in the surface layer has dealt with crack propagation and fracture (cf. Kammerhofer et al. 2013). One advantage with the predeformation technique proposed in **Paper C** is that test bars suitable for further testing are obtained. By re-machining the predeformed test bars into tubular bars, a uniform stress and strain state can be achieved. These bars can then be used to investigate how the predeformation has affected the material. Characterization of constitutive behavior, fatigue and crack propagation can be performed. In this thesis, however, the focus has been on the constitutive behavior and in particular on the evolution of yield surfaces.

Numerous studies have been carried out in the literature on the distortion of yield surfaces after plastic deformations, e.g. Naghdi et al. (1958), Phillips and Juh-Ling (1972), Moreton et al. (1978), Ishikawa and Sasaki (1989), Ishikawa (1997), Wu (2003), and Sung et al. (2011). The predeformation strains in these studies are not as large as those achieved with the predeformation method proposed in this thesis. To the knowledge of the author, yield surfaces after such large shear strains have not previously been studied.

4.1 Experimental setup

To investigate the evolution of the yield surface it must first be defined what a yield surface is. In material models, the yield surface represents the (often distinct) transition from elastic to plastic behavior. For most real materials the transition is gradual, and a distinct yield point cannot be determined. In uniaxial tensile tests, the experimentally determined yield limit is often defined as the stress at 0.2% plastic strain. At this point,

however, the material has undergone considerable plastic deformations. Much smaller offset strains can be measured with a standard extensometer.

A measure of the multiaxial plastic strain is required to determine yield surfaces. A common choice is to use the von Mises equivalent plastic strain. But using this strain measure implies that an assumption about the yield surface shape has already been made. In this thesis the plastic work w_p is used instead (following e.g. Hill and Hutchinson 1992; Hill et al. 1994), as this is independent of any assumed yield surface shape:

$$w_\mathrm{p} = \int_0^t \boldsymbol{\sigma} : \dot{\boldsymbol{\epsilon}}_\mathrm{p} \, \mathrm{d}t \tag{4.1}$$

This criterion has the additional advantage that it acts as a low-pass filter reducing the influence of noisy experimental data. The negative side of the plastic work criteria is that the connection to the uniaxial plastic strain offset is not as clear as for the effective strain approach.

In order to detect the yielding with any of the criteria discussed above, the plastic strains must be determined: Linear elasticity and additive decomposition of the strain $\boldsymbol{\epsilon}$ into an elastic and a plastic strain $\boldsymbol{\epsilon} = \boldsymbol{\epsilon}_\mathrm{e} + \boldsymbol{\epsilon}_\mathrm{p}$ is assumed. The elastic strains are given by the 4th order compliance tensor E^{-1}:

$$\boldsymbol{\epsilon}_\mathrm{p} = \boldsymbol{\epsilon} - \mathsf{E}^{-1} : \boldsymbol{\sigma} \tag{4.2}$$

In the considered experiments, $\epsilon_{z\theta}$, ϵ_{zz}, $\sigma_{z\theta}$ and σ_{zz} are measured. The remaining stress components are zero and E^{-1} in Equation (4.2) can be represented by a 2-by-2 matrix.

Two main methods are used in the literature to experimentally determine a yield surface. In the first method, one test bar is loaded sequentially in different directions, see e.g. Naghdi et al. (1958) and Sung et al. (2011). The loading is stopped once yielding is detected by e.g. a certain level of w_p. With this method, denoted yield probing, it is possible to measure the entire yield surface with only one test bar. An additional advantage with this method is that the scatter between neighboring yield points is reduced, as the same test bar is used. This improves the measurement of the local curvature of the yield surface. However, the amount of plasticity in the yield point detection must be very small to minimize the influence on subsequent measurements. This increases the measurement scatter as the relative errors in the measurements increase. Furthermore, no information about the behavior beyond the yield points is obtained.

The other approach is to use one test bar for each loading direction. This is typically used to characterize the yield surface for cold-rolled sheet metals, see e.g. Banabic et al. (2003) and Barlat et al. (2005). In those studies, the 0.2% strain offset criteria was used. While this method requires more test bars to determine the yield surface, there is no influence from previous measurements on the results. Hence, arbitrary large offset criteria can be used, and it is not necessary to determine the offset in advance.

In **Paper D** the evolution of yield surfaces is evaluated using one test bar in each loading direction. Different levels of plastic work w_p are evaluated. Only the inner surface can be considered as an approximation of a yield surface. Other surfaces of equal plastic work give further information about how the material behaves after the initial yielding. Conclusions regarding the hardening behavior can therefore be drawn as well.

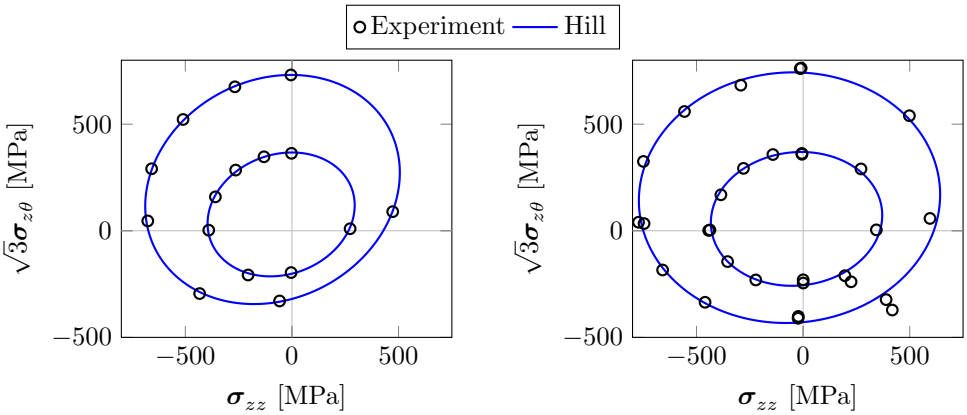

(a) *After one predeformation step* ($\gamma \approx 0.21$) (b) *After six predeformation steps* ($\gamma \approx 1.13$)

Figure 4.1: *The quadratic Hill yield criteria fitted to equal plastic work contours* ($w_\mathrm{p} = 0.025$ *and* $0.500\,\mathrm{mJ/mm^3}$) *after different levels of predeformation.*

One of the most challenging parts of **Paper D** was to manufacture the thin-walled test bars with sufficient accuracy. The procedure used to obtain a centered drilled hole is presented in detail in Meyer (2019a).

4.2 Main findings

A main goal of **Paper D** is to evaluate different anisotropic yield criteria. Three different anisotropic yield criteria are evaluated: Hill (1948), Karafillis and Boyce (1993) and Barlat et al. (2005). It turns out that the criterion by Hill (1948) is the most stable and has the best predictive ability. Figure 4.1 shows that this criterion can fit the equal plastic work contours for both the low and high plastic work limits.

5 Material modeling

Two models from **Paper C** were used to simulate 1400 cycles of 3-dimensional rolling contact loading in a wheel-rail test rig in Pletz et al. (2019). The results in Figure 5.1a show that the choice of material model has a huge influence on the predicted deformations. The calculation time was approximately 3 weeks using 10 cores on a computer cluster. For the rail samples analyzed in **Paper A** the average yearly tonnage was $15 \cdot 10^6$. For an estimated average axle load of 15 ton, this results in approximately 2800 wheel passages per day. This shows that efficient FE-modeling methodologies are needed for such simulations. Different strategies for FE-modeling are further discussed in Section 9. The need for efficient FE-models also implies that, in addition to accuracy, computational efficiency is also an important consideration for the choice of material models.

For the pearlitic steel used in this thesis, there has been quite some work on multiscale models (e.g. Allain and Bouaziz 2008; Berisha et al. 2015; Laschet et al. 2013; Lindfeldt 2014; Peng et al. 2002; Terada et al. 2004). In these works, the underlying microstructure is simulated explicitly, using either a 2d or 3d representation. Crystal plasticity, for which the individual slip systems are modeled, is typically used for the ferrite grains. Although this is often considered to be a physically-based model, the hardening of the slip systems is still largely based on phenomenological models that require parameter identification.

When simulating cyclic loading and large plastic regions, such as in Figure 5.1b, single scale phenomenological models are still the only feasible option. Many efforts have therefore been made to develop phenomenological cyclic plasticity models in the finite strain regime, see e.g. Dettmer and Reese (2004), Grilo et al. (2016), Johansson et al. (2005), Johansson et al. (2006), Menzel et al. (2005), Vladimirov et al. (2008), Wallin et al. (2003), and Wallin and Ristinmaa (2005). These are more or less motivated by the underlying mechanisms and microstructures. Larijani et al. (2013) proposed a hybrid model, obtaining a relatively fast model while still incorporating some microstructural features through an analytical homogenization (using a numerical integration on a unit sphere). The work in this thesis should be applicable for simulating repeated rolling contact loads with a reasonable computational time. The modeling is therefore limited

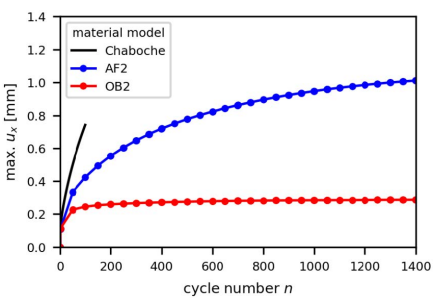

(a) *Accumulation of horizontal surface displacement.*

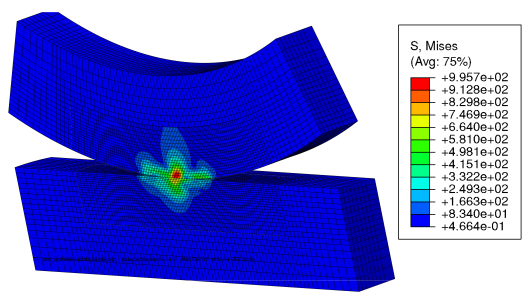

(b) *von Mises stress distribution during the rolling contact.*

Figure 5.1: *Simulations of a wheel rolling over a rail from Pletz et al. 2019.*

to single-scale phenomenological models. One exception is the crystal plasticity model evaluated in **Paper F**. The Taylor assumption of uniform strains was used for the homogenization in this case.

5.1 Model framework

In many applications the deformations and rotations are small. The finite element model can then be simplified by assuming linear kinematics. In some cases, however, it is necessary to account for the large deformations. Two examples are sheet metal forming and wheel-rail rolling contact. In the literature, there are two types of model formulations for large deformations: Hypo-models and hyper-models. Hypo-models typically extend the small strain formulations using different objective stress rates. These models are common in commercial finite element software. As an example, Abaqus (Abaqus 2013) uses the co-rotational formulation, approximated according to Hughes and Winget (1980). An advantage with this formulation is that small strain model implementations can conveniently be used. But when using von Mises plasticity with linear kinematic hardening (a special case of the Chaboche model, cf. Chaboche 1986) for simulating simple shear of a $1 \times 1 \times 1\,\text{mm}$ box, the result in Figure 5.2a is obtained. This load case, with a large shear deformation, is similar to the deformation seen at the top of the rail in Figure 1.1b. The simulation shows a non-physical oscillatory response in the reaction force, motivating the need for adopting another modeling framework. There exist hypo-models in the literature that do not show this behavior (cf. Grilo et al. 2016), but in this thesis hyper-models are adopted. The main motivation for this choice is that they are formulated in a thermodynamical framework and it is more straight forward to show that they are thermodynamically consistent (i.e. that they fulfill the second law of thermodynamics).

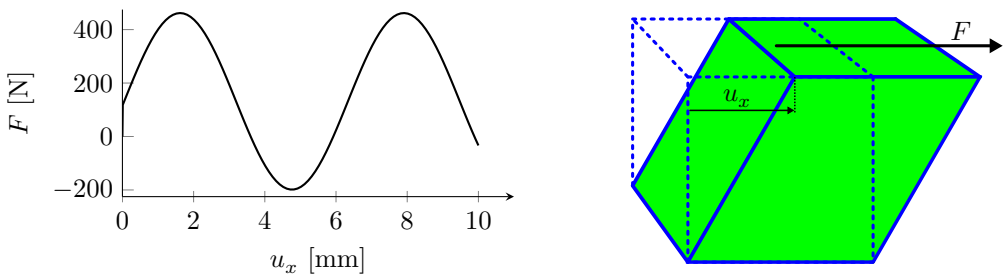

(a) *Force versus displacement.* (b) *Simple shear of a* $1 \times 1 \times 1\,\text{mm}$ *box.*

Figure 5.2: *Simulation of simple shear in Abaqus using von Mises plasticity and linear kinematic hardening.*

Two frameworks for hyperelasto-plastic models with kinematic hardening are considered in this thesis: The first was suggested by Wallin et al. (2003) and the second by Dettmer and Reese (2004). These frameworks are compared in **Paper B** where it is shown that

for the same choice of free energy they coincide.

5.2 Evolution laws for kinematic hardening

For kinematic hardening at finite strains, the choice of model framework is important to obtain a physical response, as seen in Figure 5.2. However, the evolution laws for the kinematic hardening can equally well be presented for small strains. For the exact formulations in the finite strain setting the reader is referred to **Paper C**.

Kinematic hardening is often a critical component of material models for cyclic plasticity. For pearlitic steel it can dominate over the isotropic hardening, as found in e.g. Johansson et al. (2006). To fit experimental data, multiple back-stresses are often used, see e.g. Pletz et al. (2014). The most common evolution law was proposed by Armstrong and Frederick in 1966 (Frederick and Armstrong 2007):

$$\dot{\boldsymbol{B}} = H_{\text{kin}}\dot{\lambda}\left[\boldsymbol{\nu} - \frac{3}{2}\frac{\boldsymbol{B}}{B_\infty}\right], \quad \boldsymbol{\nu} = \frac{\partial\Phi}{\partial\boldsymbol{\sigma}} \tag{5.1}$$

Here $\boldsymbol{\sigma}$ is the stress, $\boldsymbol{B}$ is the back-stress and Φ the yield function. H_{kin} is the hardening modulus, B_∞ the saturation back-stress and $\dot{\lambda}$ is the plastic multiplier. Several improvements of this evolution law have been suggested in the literature. Perhaps the most well-known is the Ohno-Wang evolution law (Ohno and Wang 1993). This model improves the control of the ratcheting rate by including another material parameter m. It also modifies the behavior during non-proportional and reversed loading:

$$\dot{\boldsymbol{B}} = H_{\text{kin}}\dot{\lambda}\left[\boldsymbol{\nu} - \frac{3}{2}\frac{\boldsymbol{B}}{B_\infty}\left(\frac{f(\boldsymbol{B})}{B_\infty}\right)^m\left\langle\frac{\boldsymbol{B}:\boldsymbol{\nu}}{B_\infty}\right\rangle\right] \tag{5.2}$$

where $f(\boldsymbol{x})$ is a function calculating the effective stress (e.g. von Mises) of the stress $\boldsymbol{x}$. The Macaulay bracket $\langle\bullet\rangle$ is defined as $\langle\bullet\rangle = 0.5(\bullet + |\bullet|)$.

While the Ohno-Wang model does incorporate an influence from non-proportional loading via the contraction $\boldsymbol{B}:\boldsymbol{\nu}$, the direction of the nonlinear evolution is the same as for the Armstrong-Frederick model. Bari and Hassan (2002) found that neither of these models could accurately predict ratcheting during non-proportional loading. Their solution was the model suggested by Delobelle et al. (1995) that combines the Armstrong-Frederick hardening with the model suggested by Burlet and Cailletaud (1986):

$$\dot{\boldsymbol{B}} = H_{\text{kin}}\dot{\lambda}\left[\boldsymbol{\nu} - \delta\frac{3}{2}\frac{\boldsymbol{B}}{B_\infty} - (1-\delta)\left(\frac{\boldsymbol{B}:\boldsymbol{\nu}}{B_\infty}\right)\boldsymbol{\nu}\right] \tag{5.3}$$

The parameter δ then controls how much of the nonlinear back-stress evolution that follows the current back-stress ($\boldsymbol{B}$) and how much that follows the current normal to the yield surface ($\boldsymbol{\nu}$). In the small strain setting, δ has no influence when the loading is proportional. This modification has been used by several authors and can greatly improve the model accuracy for non-proportional loading. A combination between the Ohno-Wang model and the Burlet-Cailletaud model was also evaluated in **Paper C**:

$$\dot{\boldsymbol{B}} = H_{\text{kin}}\dot{\lambda}\left[\boldsymbol{\nu} - \frac{\langle\boldsymbol{B}:\boldsymbol{\nu}\rangle}{B_\infty}\left(\frac{f(\boldsymbol{B})}{B_\infty}\right)^m\left(\delta\frac{3}{2}\frac{\boldsymbol{B}}{f(\boldsymbol{B})} + (1-\delta)\boldsymbol{\nu}\right)\right] \tag{5.4}$$

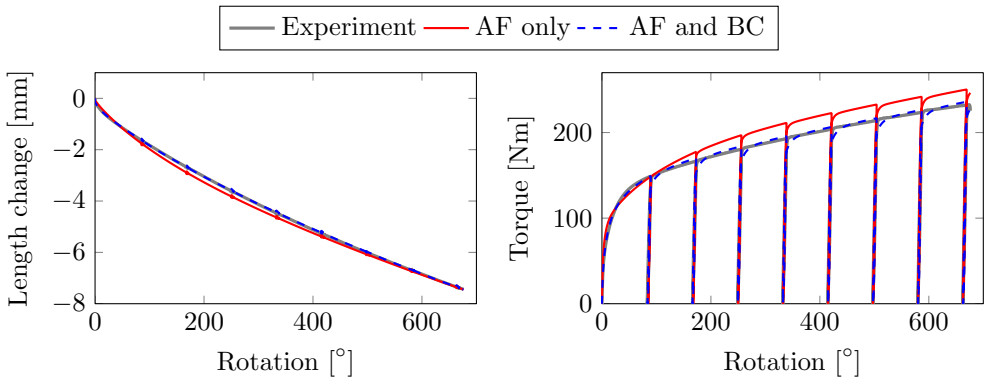

(a) *Axial response* (b) *Torsional response*

Figure 5.3: *Improvement by combining Burlet-Cailletaud (BC) with the Armstrong-Frederick (AF) kinematic hardening when simulating predeformation with* $-500\,\mathrm{MPa}$ *nominal axial stress.*

It was found that this combination only gave marginally better results compared to the combination of Burlet-Cailletaud and Armstrong-Frederick evolution laws. The main finding is that the addition of Burlet-Cailletaud hardening is required to accurately capture the material behavior during the predeformation, as seen in Figure 5.3.

5.3 Evolving yield surfaces

In **Paper D** it was observed that the yield behavior evolves from initial isotropy into anisotropy. Hence, a model that accounts for this evolution is required to accurately capture the behavior of the material in the surface layer of rails. A lot of work on constitutive models that include such an evolution has been conducted in the literature: From physically motivated crystal plasticity models to more phenomenological models. Feigenbaum and Dafalias (2007), Pietryga et al. (2012) and Shi et al. (2014) use an evolving 4th order tensor to model an anisotropic yield surface. Barlat et al. (2011), Mánik et al. (2015) and Qin et al. (2018) use a yield criterion consisting of one fixed and one fluctuating part. Finally, Dafalias (1998), Harrysson et al. (2007) and Kaiser et al. (2019) consider how the substructure evolution gives an evolving anisotropy.

From the findings in **Paper D** it seems reasonable to use a quadratic Hill-type yield function as it can describe the experimental findings well. Such a yield function, Φ can, in general, be written as:

$$\Phi = \sqrt{\boldsymbol{\sigma}_{\mathrm{red}} : \mathsf{C} : \boldsymbol{\sigma}_{\mathrm{red}}} - R \tag{5.5}$$

where $\boldsymbol{\sigma}_{\mathrm{red}} = \boldsymbol{\sigma} - \boldsymbol{B}$ is the reduced stress and R is the current isotropic yield limit including the isotropic hardening. The fourth-order tensor C describes the anisotropy of the yield criterion and evolves with plastic deformations. The models in this section will

also be formulated in a small strain setting for clarity. The corresponding finite strain formulations are given in **Paper F**.

In **Paper F** two different models with an evolving C are evaluated. For the first model, based on Shi et al. (2014), the evolution of C is split into a dynamic (C_d) and a latent (C_l) part. The dynamic part is responsible for hardening in the loading direction (also called self-hardening), while the latent part controls the hardening in the directions perpendicular to the loading (also called cross-hardening):

$$\mathsf{C} = \frac{3}{2}\left((1-b_\mathrm{d}-b_\mathrm{l})\mathsf{I}^\mathrm{dev} + b_\mathrm{d}\mathsf{C}_\mathrm{d} + b_\mathrm{l}\mathsf{C}_\mathrm{l}\right) \tag{5.6}$$

$$\dot{\mathsf{C}}_\mathrm{d} = -\dot{\lambda}c_\mathrm{d}\left(\mathsf{N}:\mathsf{C}_\mathrm{d}\right)\mathsf{N}, \quad \mathsf{N} = \boldsymbol{N}\otimes\boldsymbol{N}, \quad \boldsymbol{N} = \frac{\boldsymbol{\sigma}_\mathrm{red}^\mathrm{dev}}{\left|\left|\boldsymbol{\sigma}_\mathrm{red}^\mathrm{dev}\right|\right|} \tag{5.7}$$

$$\dot{\mathsf{C}}_\mathrm{l} = -\dot{\lambda}c_\mathrm{l}\left(\mathsf{N}_\perp:\mathsf{C}_\mathrm{l}\right)\mathsf{N}_\perp, \quad \mathsf{N}_\perp = \mathsf{I}^\mathrm{dev} - \mathsf{N} \tag{5.8}$$

where b_d, b_l, c_d and c_l are material parameters.

The yield function in the second model, based on Qin et al. (2018), consists of a fixed and a fluctuating part:

$$\Phi = \left(g_1 f_\mathrm{fixed}\left(\boldsymbol{\sigma}_\mathrm{red}\right)^q + (1-g_1)\left(\sqrt{\frac{3}{2}}\frac{|\boldsymbol{P}:\boldsymbol{\sigma}_\mathrm{red}|}{||\boldsymbol{P}||}\right)^q\right) - R \tag{5.9}$$

where f_fixed is a measure of effective stress that does not evolve with deformations. The microstructure deviator $\boldsymbol{P}$ and the scaling g_1 evolve with the deformation. For the case of f_fixed being the standard von Mises effective stress and the exponent $q = 2$, Equation (5.9) can be written as Equation (5.5) with C according to:

$$\mathsf{C} = \frac{3}{2}\left[g_1\mathsf{I}^\mathrm{dev} + (1-g_1)\frac{\boldsymbol{P}}{||\boldsymbol{P}||}\otimes\frac{\boldsymbol{P}}{||\boldsymbol{P}||}\right] \tag{5.10}$$

For this special case, which is used in **Paper F**, this model also has a quadratic yield function.

An alternative approach to the phenomenological models described above is to directly model the behavior of each grain. Using the crystal plasticity formulation in **Paper F**, fewer material parameters are used compared to the other models. However, the computational cost is significantly higher. A full multiscale model, in which the actual microstructure is resolved, is not feasible. Hence, the Taylor (Voigt) assumption of equal strains in all grains is adopted to homogenize the response from 32 uniform grain orientations. The yield surfaces for the individual grains have sharp corners. But as many grains are simulated, and a viscoplastic regularization is used, the resulting homogenized yield surface is smooth.

The crystal plasticity approach was not successful in describing the material behavior. It was outperformed by the base model that used the von Mises yield criterion without any distortional hardening. The models from Shi et al. (2014) and Qin et al. (2018) were, on the other hand, quite successful in fitting the experimental behavior. Figures 5.4a and 5.4b show that the Shi model could model the predeformation quite accurately. The

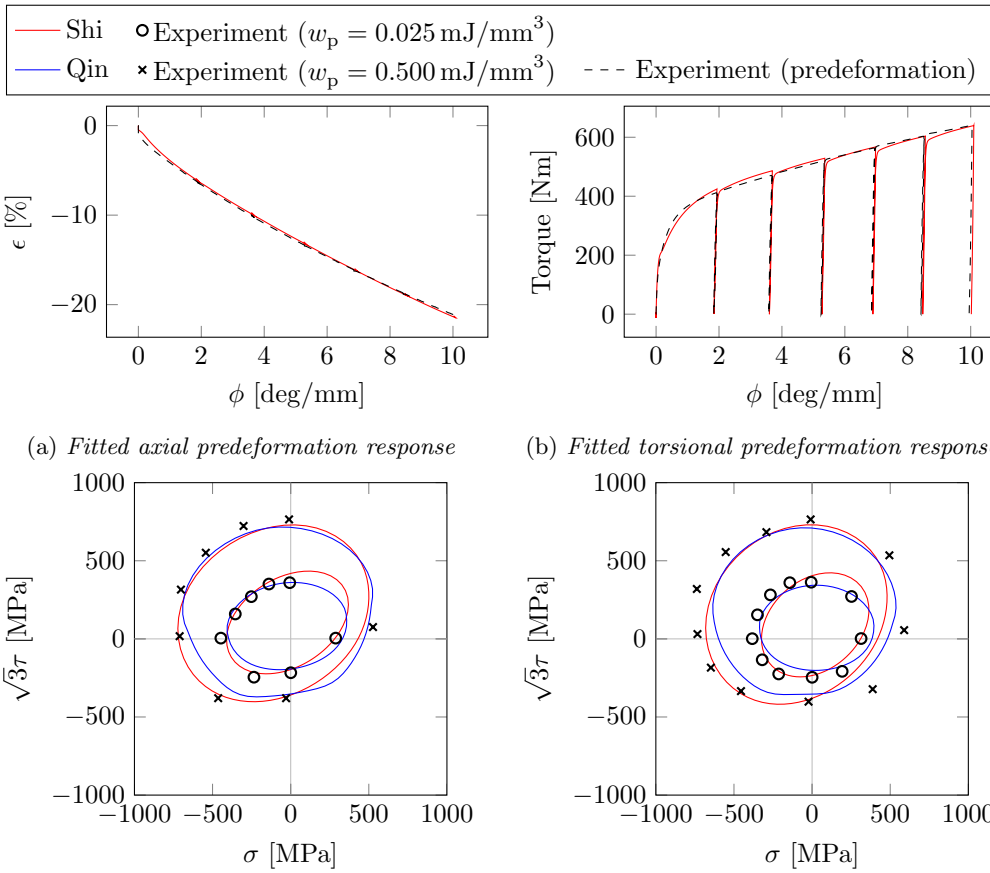

(a) *Fitted axial predeformation response*

(b) *Fitted torsional predeformation response*

(c) *Fitted yield response after 3 predeformation steps*

(d) *Predicted yield response after 6 predeformation steps*

Figure 5.4: *Response for the Shi and Qin models*

fits were not as good for the Qin model, but still quite good. In Figure 5.4c the fitted yield surfaces after 3 predeformation steps are shown for these models, and both fit the experimental yield points rather well. However, there is still much room for improvement in the predictive ability for these models as is shown in Figure 5.4d. The model based on Shi et al. (2014) suffers from some numerical issues as stringent bounds of allowable parameter values (e.g. to ensure a convex yield surface) have not been determined. This is further discussed in Appendix C in **Paper F**.

6 Simulation of experiments

The results in e.g. Bari and Hassan (2002) and Johansson et al. (2006) show that multiaxial, non-proportional loading is required to fully characterize the cyclic material behavior. Multi-axial loading is also needed to characterize anisotropy. Different types of multi-axial experiments are used in the literature: The two most common are the biaxial tensile test using cruciform specimens and axial-torsion-pressure loading of tubular test bars. Biaxial tension tests require a good design of the cruciform specimens to get an accurate calculation of the stresses. Banabic et al. (2003) estimated errors in their calculated stresses to be between 2% and 4%. This test method is particularly well suited for sheet metal testing. For the axial-torsion-pressure loading, it is most common to combine axial loading with either torsional or pressure loading. Some authors have combined all three loading types allowing greater flexibility in the loading, see e.g. Bocher et al. (2001) and Sung et al. (2011). The pressure and torsional loading do not result in a fully homogeneous deformation field: The strains depend on the radius. The error due to this is minimized by using thin-walled test bars. As the wall thickness decreases, however, the cost and relative geometrical errors for the test bars increase. The loading of a solid cylindrical test bar was simulated in **Paper C**. This setup is described in Subsection 6.1. In **Paper E** an efficient simulation methodology for axial-torsion-pressure loading is proposed. The main ideas of this methodology are presented in Subsection 6.2. Finally, the extension of this methodology to include material removal is presented in Subsection 6.3.

6.1 2D axisymmetric simulation

The mechanical extensometer was unable to measure the large strains during the predeformation. Hence, the rotation and displacement of the entire test bar were used in **Paper C**. They were measured by the position and rotation sensors of the testing machine. The compensation to remove the influence the machine frame deflections is described in Appendix A in **Paper C**.

To simulate the full test bar, quadratic 2D generalized axisymmetric elements (CGAX8R) in Abaqus (Abaqus 2013) were used. Parameter identification was performed by calling Abaqus from an optimization routine in MATLAB. While this method worked rather well, there are two main drawbacks with this method:

- The simulation time of the predeformation is quite long. Also, there is an overhead time required to initiate the Abaqus code.
- Further modeling errors are introduced as the entire test bar is modeled. The strain distribution along the test bar is not measured in the experiments.

Figure 6.1 shows the residual shear stresses after the predeformation in **Paper C**. No gradient in the axial direction is observed in the central part of the gauge section. This shows that it is possible to only consider the local strains in the gauge section. A simulation methodology utilizing this feature is described in the next subsection.

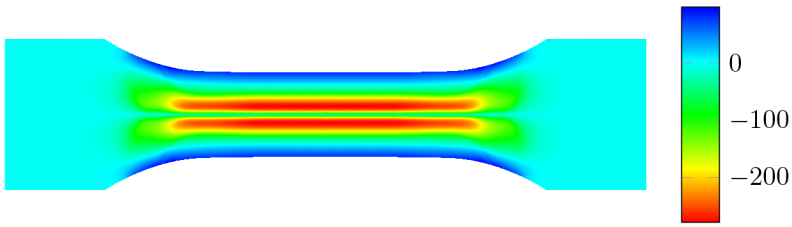

Figure 6.1: *Calculated residual shear stresses [*MPa*] after the predeformation in* ***Paper C***

6.2 Axial-Torsion-Pressure (ATP) simulation

The drawbacks of the method described above motivate the development of an improved simulation methodology. As was also described above, it is sufficient to only simulate the local strains in the gauge section. For this to be possible, however, it is necessary to measure these strains experimentally. In **Paper E**, as previously mentioned, this is accomplished by using DIC.

A cylindrical coordinate system $R - \Theta - Z$ with the radius R, angle Θ and axial coordinate Z is introduced. From Figure 6.1 it can be motivated that the derivatives with respect to the axial coordinate are zero in the middle of the gauge section, i.e. $\partial \bullet / \partial Z = 0$. Furthermore, assuming that the gauge section (with a constant cross-sectional area) is sufficiently long, it can be assumed that straight radial lines remain straight and radial. This allows the 2D finite element model to be reduced to a 1D formulation, significantly reducing the simulation time. These kinematic assumptions are illustrated in Figure 6.2.

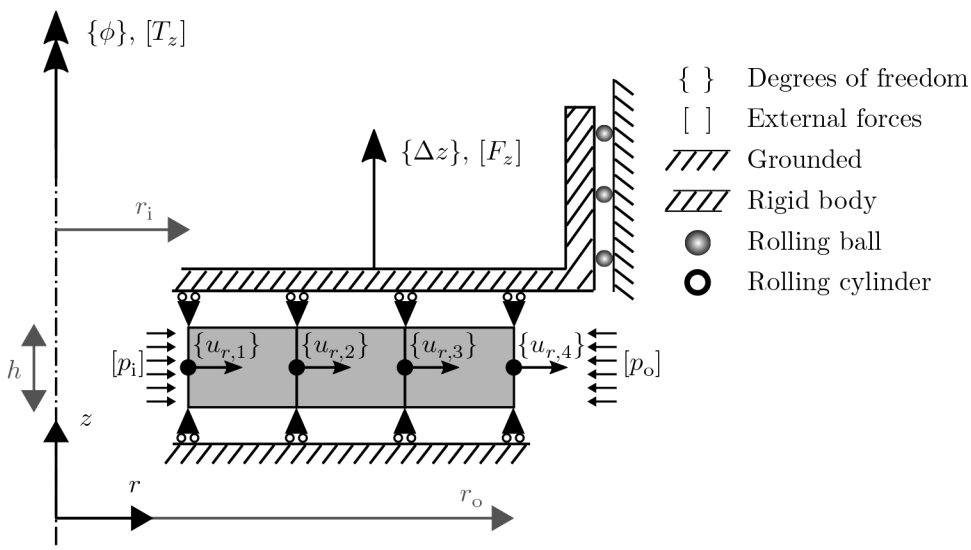

Figure 6.2: *Kinematic assumptions and degrees of freedom for the ATP simulation*

The kinematic assumptions discussed above can be simulated by using a single element row of the generalized axisymmetric elements in Abaqus. This method was compared to using the 1D software implementation in the software `matmodfit` (Meyer 2019b) in **Paper E**. The results show that the 1D implementation is between 100 and 200 times faster than the equivalent Abaqus simulation. Parameter identification requires many simulations with different material parameter values. Hence, the simulation time for each set of parameter values is very important.

6.3 Material removal simulation

To simulate the experiment from **Paper D**, the ATP simulation methodology is extended in **Paper F**: The process of removing material and obtaining a tubular, predeformed test bar is included. From the experiments, the dimensions of the tubular test bar are only known in the relaxed state after the re-machining. Due to residual stresses, the geometry changes during the relaxation occurring when the material is removed. An iterative strategy to determine the mesh for the re-machined test bar is therefore presented in **Paper F** and illustrated in Figure 6.3.

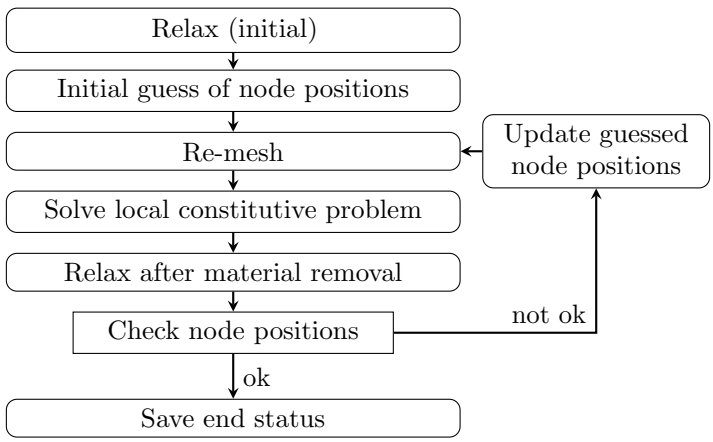

Figure 6.3: *The steps in the simulation of the material removal procedure*

During the re-meshing stage, the material state is interpolated from the old to the new integration points. Local equilibrium in the constitutive problem in each integration point is typically not fulfilled after the interpolation. Hence, this is solved as a new load step in the material. In cases when a solution is not obtained, a sub-stepping method is applied. This implies interpolating the state to intermediate points to reduce the perturbation of the local equilibrium. A smaller perturbation results in a better initial guess for the solution of the local problem, increasing the probability of obtaining a converged solution. With this additional method, it was possible to simulate the experiments with quite coarse meshes, as studied in Appendix A in **Paper F**. For the crystal plasticity modeling with more than 4000 state variables, however, convergence is still a problem in some cases.

7 Parameter identification

A task requiring a lot of the work in **Paper C** - **Paper F** is parameter identification. While the development of methods for this is not a focus of this thesis, a lot of the work relies on such methods. This chapter contains a brief discussion about the methods utilized in the appended papers.

The parameters for simple models, such as linear elasticity can be identified directly by linear regression. However, as explained by Mahnken (2014), for advanced material models, such as those used in this thesis, numerical optimization is required for parameter identification. In the appended papers the chosen parameter identification methodology consists of the following steps:

- Define an objective function $f(\boldsymbol{p})$
- Generate a full set $\mathbb{S}_{\text{full}}$ of starting guesses $\boldsymbol{p}_i$ ($i \in \mathbb{S}_{\text{full}}$) for the parameters.
- Evaluate objective function $f(\boldsymbol{p}_i)$ for each $i \in \mathbb{S}_{\text{full}}$. Choose the set $\mathbb{S}_{\text{red}} \subset \mathbb{S}_{\text{full}}$ with starting guesses to optimize from.
- Minimize the objective function with chosen optimization algorithm for each starting guess in $\mathbb{S}_{\text{red}}$
- Choose the optimized parameter values $\boldsymbol{p}$ resulting in the lowest objective function value
- Evaluate the ability of the material model with the chosen parameter values to predict the experimental data not used in the objective function

The choice of the objective function will have a significant influence on the results. In general, the objective function consists of a least-square fitting error:

$$f(\boldsymbol{p}) = \sum_i \left(y_i^{\text{exp}} - y_i^{\text{sim}}(\boldsymbol{p}) \right)^2 \tag{7.1}$$

where y_i^{exp} are the experimentally measured data points and $y_i^{\text{sim}}(\boldsymbol{p})$ are the corresponding simulated points (as a function of the material parameters $\boldsymbol{p}$). An important choice is which experiments to include in the objective function. Some data should be retained to evaluate the predictive ability of the model. When the objective function accounts for different experiments and different measured quantities the scaling of each experiment is also an important issue. In **Paper C**, heuristically chosen scaling factors were employed. This was improved in **Paper D** - **Paper F**, where the terms in the objective function were normalized by the range of the experimental data. In **Paper E** a special objective function for ratcheting experiments was proposed: It separates the error in the cycle shape and the strain accumulation.

In **Paper C**, **Paper E** and **Paper F** it was clear that a large spread of the starting guesses is important to identify good final parameter values. Latin hypercube sampling was therefore used to distribute a high number of initial parameter values. The objective

function for these values was then evaluated. A certain number of values resulting in the lowest objective function value were finally chosen for minimization.

A lot of different optimization algorithms are used for parameter identification in the literature. These can be grouped into deterministic and stochastic algorithms. Stochastic algorithms are usually considered to be better at finding the global optimum. But they typically require a higher number of objective function evaluations (Mahnken 2014). Some authors have used stochastic algorithms directly, e.g. Li et al. (2017). However, it is more common to combine stochastic algorithms with local, deterministic, algorithms to increase the convergence rate, see e.g. Chaparro et al. (2008) and De-Carvalho et al. (2011). A stochastic method by Runarsson and Yao 2005 was tried out in **Paper E**. But using the deterministic Nelder-Mead simplex algorithm (Nelder and Mead 1965) with multiple starting guesses resulted in better optima. From the experience of the author of this thesis, the simplex algorithm works well compared to other methods for parameter identification. In **Paper F** multiple re-starts of the simplex were used to reduce the risk of getting trapped in local minima. Using the Subplex method (Rowan 1990) should also help to alleviate this problem, but the standard simplex algorithm performed better. Hence, the simplex method is used throughout this thesis for parameter identification. As previously described, however, a high number of initial guesses is required to obtain a good best optimum.

In **Paper F** it was found that a different seed for the Latin Hypercube sampling did not give the same best optimum. This implies that it can never be known if a better set of parameter values exists. An interesting approach is to use smaller portions of the experiments to identify certain parameters, see e.g. Qin et al. (2018). For this to be effective the formulation of the material model and the available experiments must be matched. When the purpose is to compare models, however, there is a risk of having a biased method favoring a certain model. The identification of material parameters for complex models is still an open research question.

8 Discussion

Three aims for this thesis were presented in Subsection 1.1. In this section the fulfillment of these aims is discussed.

1. **Obtain test bars with similar properties as the surface layer of rails**

   In **Paper A** it was shown that the obtained test bars have similar properties as the material in the surface layer of railway rails. The top 0.05 mm could not be represented with test bars obtained with this method. To achieve such large strains, other methods, e.g. HPT, are required. However, the proposed method makes it possible to test cyclic, multiaxial loading of predeformed test bars. This is difficult to accomplish for samples deformed by the HPT method.

   The current requirements for railway grade materials are put on the properties of the virgin material (e.g. yield limit, fracture toughness). But, to measure the actual performance in service, it might be more relevant to consider the material properties after large strains have accumulated. The predeformation method can therefore be a first step towards having more relevant demands on rail materials.

2. **Determine how the behavior of the material in the surface layer of rails evolves**

   Paper D extends the predeformation method by including the re-machining of the predeformed test bars into tubular bars. The evolution of the monotonic plastic behavior was then evaluated after different levels of predeformation. This is one example of the type of evaluations that can be performed using the developed predeformation method. The experiments also included cyclic loading after the monotonic loading that was presented in **Paper D** and then used in **Paper F**. This data can in the future be used to analyze and calibrate models for cyclic plasticity and low cycle fatigue. Due to the surface roughness of the drilled holes (see Meyer 2019a), the fatigue results might have too much statistical variation.

   The results in **Paper D** show that the quadratic Hill yield criterion can fit the measured yield surfaces well. This finding can support the development of constitutive models, and it implies that a simple quadratic yield surface can be used.

3. **Model the behavior of the material in the surface layer of rails.**

   The predeformation was first modeled in **Paper C**. In **Paper E** a new simulation methodology for axial, torsion and pressure (ATP) loading was presented. In combination with DIC strain measurements, it enabled a very efficient simulation of the predeformation. In **Paper E** this framework was first extended to include material removal such that the re-machining of the test bars could be simulated as well. The ATP simulation methodology has also been used by Esmaeili (2019).

   Paper C shows that the mechanical response during the predeformation can be modeled with an isotropic yield surface. However, advanced kinematic hardening laws were required, strengthening the results reported in the literature for nonproportional loading. Advanced material models with distortional hardening were used in **Paper**

F: Both the evolving anisotropic yield surface and the multiaxial stress-strain response were evaluated. The two models that used a quadratic Hill-type yield criterion performed best.

9 Future work

9.1 Finite element modeling

As briefly mentioned earlier, Pletz et al. (2019) simulated the elastoplastic rail-wheel rolling contact using material models from **Paper C**. The approximate simulation time was roughly 6 weeks per day of traffic. This shows that this model cannot be used to simulate long-term degradation of rails and that there is a need to develop faster models. These simulations could become faster by using an Arbitrary Lagrangian-Eulerian (ALE) description, as advocated in e.g. Draganis et al. (2014). Further speed-up could be achieved by using simple static condensation or more advanced numerical model order reduction methods (see e.g. Michel and Suquet 2003; Radermacher and Reese 2014). An efficient alternative approach is to use a simplified 2D FE-simulation where the load is applied as a pressure distribution, see e.g. Andersson et al. (2015). Furthermore, Skrypnyk et al. (2019a) developed a metamodel for this pressure distribution that was trained by 3D elastoplastic indentation simulations. Finally, by using cyclic extrapolation techniques it is not necessary to simulate each load cycle (see e.g. Johansson and Ekh 2007; Skrypnyk et al. 2019b). However, independently of the chosen techniques, an accurate material model is an important component of the FE modeling.

9.2 Material modeling

As shown in **Paper F**, more work is still required to be able to accurately capture the evolving yield surfaces in the rail steel. As a first step, improvements to e.g. the Shi and Qin models should be considered. In **Paper F**, the cyclic loading following the monotonic load has not been accounted for. This is a natural extension of that work. A good model should be able to capture the cyclic behavior of the undeformed as well as of the predeformed material. The cyclic experiments contain non-proportional loading that is similar to the rolling contact loading.

As was discussed in Section 7, the calibration of the material models is also an important topic. It would therefore be advantageous with model formulations such that individual material parameters can be identified directly from the experiment using e.g. linear regression. This is currently only done for the elastic parameters. If more parameters can be removed from the inverse modeling, it would likely result in a more robust parameter identification scheme.

9.3 Damage and fatigue

In addition to the plastic behavior considered in this thesis, damage and fatigue should be included in the modeling. An important requirement of the deterioration of rail materials is to account for the degradation of the material. This could be modeled in a coupled sense as done in damage modeling (see e.g. Gurson 1977; Lemaitre 1985). An alternative approach is to use a decoupled approach that is common in fatigue evaluation (see e.g.

You and Lee 1996). The latter approach has the advantage of lower computational cost as the evaluation can be done as a post-processing step. In such a decoupled scheme the influence of the degradation on the stress-strain behavior is neglected. Cracks are typically small in the main part of the fatigue life and thus have a small influence on the stress-strain response. Due to the potential reduction of the computational cost, this simplification might be worth considering.

The predeformation experiments conducted in the preparation of **Paper C** include several repeated experiments as well as variation in the loading rate, the rotation increment and the axial loading. These experiments could be used to evaluate different crack initiation criteria suitable for the rolling contact loading. The experimental methodology to obtain predeformed tubular test bars in **Paper D** can also be used to evaluate low cycle fatigue initiation criteria: These should take the effect of the accumulated shear strains into account. Furthermore, the effect on crack propagation resistance and growth direction could be evaluated.

9.4 Rate sensitivity and thermal effects

Finally, the work in this thesis has been limited to low strain rates at room temperature. Esmaeili (2019) investigated tread braking of railway wheels, for which the rate and thermal effects become very important. Although there is no large-scale temperature increase during regular rolling contact, the loading rate is very high compared to that of the experiments: The elastoplastic contact patch calculated in Pletz et al. (2019) was approximately 20 mm long. A train speed of 100 km/h then results in a load frequency of about 1.4 kHz. This can be compared to typical load frequencies between 0.25 and 5 Hz in low cycle fatigue testing. Using the frequencies in the higher end of this spectrum results in a significant temperature increase.

Some tests were carried out on the rate sensitivity of the material. In **Paper F** the rate-dependent crystal plasticity model is calibrated towards a stress relaxation. However, when testing the stabilized hysteresis loop after 50 cycles, no rate dependency can be observed despite almost one order of magnitude difference between the rates. These findings, combined with the extreme loading rates in the application, show that the rate dependency and thermal effects require more thorough investigations.

References

Abaqus (2013). *Abaqus Theory Guide*. 6.13. Providence, RI, USA: Dassault Systèmes.

Allain, S. and Bouaziz, O. (2008). Microstructure based modeling for the mechanical behavior of ferrite-pearlite steels suitable to capture isotropic and kinematic hardening. *Materials Science and Engineering A* 496 (1-2), 329–336.

Alwahdi, F. A. M., Kapoor, A., and Franklin, F. J. (2013). Subsurface microstructural analysis and mechanical properties of pearlitic rail steels in service. *Wear* 302 (1-2), 1453–1460.

Andersson, R. et al. (2015). An efficient approach to the analysis of rail surface irregularities accounting for dynamic train–track interaction and inelastic deformations. *Vehicle System Dynamics* 53 (11), 1667–1685.

Banabic, D. et al. (2003). Non-quadratic yield criterion for orthotropic sheet metals under plane-stress conditions. *International Journal of Mechanical Sciences* 45 (5), 797–811.

Bari, S. and Hassan, T. (2002). An advancement in cyclic plasticity modeling for multiaxial ratcheting simulation. *International Journal of Plasticity* 18 (7), 873–894.

Barlat, F. et al. (2005). Linear transfomation-based anisotropic yield functions. *International Journal of Plasticity* 21 (5), 1009–1039.

Barlat, F. et al. (2011). An alternative to kinematic hardening in classical plasticity. *International Journal of Plasticity* 27 (9), 1309–1327.

Berisha, B. et al. (2015). Multiscale modeling of failure initiation in a ferritic-pearlitic steel. *Acta Materialia* 100, 191–201.

Bocher, L. et al. (2001). Mechanical and microstructural investigations of an austenitic stainless steel under non-proportional loadings in tension-torsion-internal and external pressure. *International Journal of Plasticity* 17 (11), 1491–1530.

Burlet, H. and Cailletaud, G. (1986). Numerical techniques for cyclic plasticity at variable temperature. *Engineering Computations* 3 (2), 143–153.

Cannon, D. F. et al. (2003). Rail defects: An overview. *Fatigue and Fracture of Engineering Materials and Structures* 26 (10), 865–886.

De-Carvalho, R., Valente, R., and Andrade-Campos, A. (2011). Optimization strategies for non-linear material parameters identification in metal forming problems. *Computers & Structures* 89 (1-2), 246–255.

Chaboche, J. (1986). Time-independent constitutive theories for cyclic plasticity. *International Journal of Plasticity* 2 (2), 149–188.

Chaparro, B. et al. (2008). Material parameters identification: Gradient-based, genetic and hybrid optimization algorithms. *Computational Materials Science* 44 (2), 339–346.

Dafalias, Y. F. (1998). Plastic spin: necessity or redundancy? *International Journal of Plasticity* 14 (9), 909–931.

Delobelle, P., Robinet, P., and Bocher, L. (1995). Experimental study and phenomenological modelization of ratchet under uniaxial and biaxial loading on an austenitic stainless steel. *International Journal of Plasticity* 11 (4), 295–330.

Dettmer, W. and Reese, S. (2004). On the theoretical and numerical modelling of Armstrong-Frederick kinematic hardening in the finite strain regime. *Computer Methods in Applied Mechanics and Engineering* 193 (1), 87–116.

Draganis, A., Larsson, F., and Ekberg, A. (2014). Finite element analysis of transient thermomechanical rolling contact using an efficient arbitrary Lagrangian-Eulerian description. *Computational Mechanics* 54 (2), 389–405.

EIM-EFRTC-CER WORKING GROUP (2012). *Track Maintenance & Renewal*. URL: `http://www.cer.be/sites/default/files/publication/2353_7473-11_MARKET_STRATEGY_A4_FINAL.pdf`.

Esmaeili, A. (2019). "Modelling of cyclic and viscous behaviour of thermomechanically loaded pearlitic steels; Application to tread braked railway wheels". PhD Thesis. Chalmers University of Technology.

Feigenbaum, H. P. and Dafalias, Y. F. (2007). Directional distortional hardening in metal plasticity within thermodynamics. *International Journal of Solids and Structures* 44 (22-23), 7526–7542.

Frederick, C. O. and Armstrong, P. J. (2007). A mathematical representation of the multiaxial Bauschinger effect. *Materials at High Temperatures* 24 (1), 1–26.

Gavriljuk, V. (2002). Comment on "Cementite decomposition in heavily drawn pearlite steel wire". *Scripta Materialia* 46 (2), 175–177.

Grilo, T. J. et al. (2016). A finite strain constitutive model for non-quadratic yield criteria and nonlinear kinematic/isotropic hardening: application to sheet metal forming. *Archive of Applied Mechanics* 86 (1), 1–17.

Gurson, A. L. (1977). Continuum theory of ductile rupture by void nucleation and growth: Part 1 - yield criteria and flow rules for porous ductile media. *Journal of Engineering Materials and Technology, Transactions of the ASME* 99 (1), 2–15.

Harrysson, M., Harrysson, A., and Ristinmaa, M. (2007). Spatial representation of evolving anisotropy at large strains. *International Journal of Solids and Structures* 44 (10), 3514–3532.

Hill, R. (1948). A Theory of the Yielding and Plastic Flow of Anisotropic Metals. *Proceedings of the Royal Society A: Mathematical, Physical and Engineering Sciences* 193 (1033), 281–297. arXiv: `1108.0910`.

Hill, R., Hecker, S. S., and Stout, M. G. (1994). An investigation of plastic flow and differential work hardening in orthotropic brass tubes under fluid pressure and axial load. *International Journal of Solids and Structures* 31 (21), 2999–3021.

Hill, R. and Hutchinson, J. W. (1992). Differential Hardening in Sheet Metal Under Biaxial Loading: A Theoretical Framework. *Journal of Applied Mechanics* 59 (2S), S1–S9.

Hohenwarter, A. et al. (2011). Effect of large shear deformations on the fracture behavior of a fully pearlitic steel. *Metallurgical and Materials Transactions A: Physical Metallurgy and Materials Science* 42 (6), 1609–1618.

Hughes, T. J. R. and Winget, J. (1980). Finite rotation effects in numerical integration of rate constitutive equations arising in large-deformation analysis. *International Journal for Numerical Methods in Engineering* 15 (12), 1862–1867.

Ishikawa, H. (1997). Subsequent Yield Surface Probed From Its Current Center. *International Journal of Plasticity* 13 (6-7), 533–549.

Ishikawa, H. and Sasaki, K. (1989). Stress-Strain Relations of SUS304 Stainless Steel After Cyclic Preloading. *Journal of Engineering Materials and Technology* 111, 417–423.

Izotov, V. I. et al. (2007). Influence of the pearlite fineness on the mechanical properties, deformation behavior, and fracture characteristics of carbon steel. *The Physics of Metals and Metallography* 103 (5), 519–529.

Johansson, G. (2006). "On the modeling of large ratcheting strains and anisotropy in pearlitic steel". PhD thesis. Chalmers University of Technology.

Johansson, G., Ahlström, J., and Ekh, M. (2006). Parameter identification and modeling of large ratcheting strains in carbon steel. *Computers and Structures* 84 (15-16), 1002–1011.

Johansson, G. and Ekh, M. (2007). On the modeling of large ratcheting strains with large time increments. *Engineering Computations* 24 (3), 221–236.

Johansson, G., Ekh, M., and Runesson, K. (2005). Computational modeling of inelastic large ratcheting strains. *International Journal of Plasticity* 21 (5), 955–980.

Johnson, K. (1989). The Strenght of Surfaces in Rolling Contact. *Journal of Mechanical Engineering Science* 203 (December 1988), 151–163.

Kaiser, T. et al. (2019). A Covariant Formulation of Finite Plasticity with Plasticity-induced Evolution of Anisotropy: Modeling, Algorithmics, Simulation, and Comparison to Experiments. *International Journal of Solids and Structures*.

Kammerhofer, C. et al. (2013). Influence of morphology and structural size on the fracture behavior of a nanostructured pearlitic steel. *Materials Science and Engineering A* 585, 190–196.

Karafillis, A. and Boyce, M. (1993). A general anisotropic yield criterion using bounds and a transformation weighting tensor. *Journal of the Mechanics and Physics of Solids* 41 (12), 1859–1886.

Larijani, N., Johansson, G., and Ekh, M. (2013). Hybrid micro-macromechanical modeling of anisotropy evolution in pearlitic steel. *European Journal of Mechanics - A/Solids* 38, 38–47.

Larijani, N. et al. (2014). The effect of anisotropy on crack propagation in pearlitic rail steel. *Wear* 314 (1-2), 57–68.

Laschet, G. et al. (2013). Derivation of anisotropic flow curves of ferrite-pearlite pipeline steel via a two-level homogenisation scheme. *Materials Science and Engineering: A* 566, 143–156.

Lemaitre, J. (1985). A Continuous Damage Mechanics Model for Ductils Fracture. *Transaction of the ASME, Journal of engineering materials and technology* 107 (January 1985), 83–89.

Li, Y. et al. (2012). Evolution of strength and microstructure during annealing of heavily cold-drawn 6.3GPa hypereutectoid pearlitic steel wire. *Acta Materialia* 60 (9), 4005–4016.

Li, Y. et al. (2017). Identification of advanced constitutive model parameters through global optimization approach for DP780 steel sheet. *Procedia Engineering* 207, 125–130.

Lidén, T. and Joborn, M. (2016). Dimensioning windows for railway infrastructure maintenance: Cost efficiency versus traffic impact. *Journal of Rail Transport Planning & Management* 6 (1), 32–47.

Lindfeldt, E. (2014). "On multiscale modeling of pearlitic steel". PhD thesis. Chalmers University of Technology.

Mahnken, R. (2014). "The History of Theoretical, Material and Computational Mechanics - Mathematics Meets Mechanics and Engineering". *The History of Theoretical, Material and Computational Mechanics - Mathematics Meets Mechanics and Engineering*. Ed. by E. Stein. Vol. 1. Berlin, Heidelberg: Springer, pp. 229–247. DOI: 10.1007/978-3-642-39905-3. URL: http://link.springer.com/10.1007/978-3-642-39905-3.

Mánik, T., Holmedal, B., and Hopperstad, O. S. (2015). Strain-path change induced transients in flow stress, work hardening and r-values in aluminum. *International Journal of Plasticity* 69, 1–20.

Marshall, M. B. et al. (2006). Experimental characterization of wheel-rail contact patch evolution. *Journal of Tribology* 128 (3), 493–504.

Menzel, A. et al. (2005). A framework for multiplicative elastoplasticity with kinematic hardening coupled to anisotropic damage. *International Journal of Plasticity* 21 (3), 397–434.

Meyer, K. A. (2019a). *Drilling of predeformed test bars*. Tech. rep. Gothenburg: Chalmers University of Technology, pp. 1–6. DOI: 10.13140/RG.2.2.31742.54082/1.

Meyer, K. A. (2019b). *matmodfit*. URL: https://github.com/KnutAM/matmodfit.

Michel, J. and Suquet, P. (2003). Nonuniform transformation field analysis. *International Journal of Solids and Structures* 40 (25), 6937–6955.

Moreton, D. N., Moffat, D. G., and Hornby, R. P. (1978). Techniques for investigating the yield surface behavior of pressure-vessel materials. *Journal of Strain Analysis* 13 (3), 185–191.

Naghdi, P. M., Essenburg, F., and Koff, W. (1958). An experimental study of initial and subsequent yield surfaces in plasticity. *J. Appl. Mech.* 25 (2), 201–209.

Nelder, J. A. and Mead, R. (1965). A Simplex Method for Function Minimization. *The Computer Journal* 7 (4), 308–313.

Nikas, D., Zhang, X., and Ahlström, J. (2018). Evaluation of local strength via microstructural quantification in a pearlitic rail steel deformed by simultaneous compression and torsion. *Materials Science and Engineering: A* 737, 341–347.

Ohno, N. and Wang, J.-D. (1993). Kinematic hardening rules with critical state of dynamic recovery, part I: formulation and basic features for ratchetting behavior. *International Journal of Plasticity* 9 (3), 375–390.

Pau, M., Aymerich, F., and Ginesu, F. (2002). Distribution of contact pressure in wheel–rail contact area. *Wear* 253 (1-2), 265–274.

Peng, X., Fan, J., and Yang, Y. (2002). A microstructure-based description for cyclic plasticity of pearlitic steel with experimental verification. *International Journal of Solids and Structures* 39 (2), 419–434.

Phillips, A. and Juh-Ling, T. (1972). The effect of loading path on the yield surface at elevated temperatures. *International Journal of Solids and Structures* 8 (4), 463–474.

Pietryga, M. P., Vladimirov, I. N., and Reese, S. (2012). A finite deformation model for evolving flow anisotropy with distortional hardening including experimental validation. *Mechanics of Materials* 44, 163–173.

Pippan, R. and Hohenwarter, A. (2016). The importance of fracture toughness in ultrafine and nanocrystalline bulk materials. *Materials Research Letters* 3831 (April), 1–10.

Pletz, M. et al. (2014). Multi-scale finite element modeling to describe rolling contact fatigue in a wheel–rail test rig. *Tribology International* 80, 147–155.

Pletz, M. et al. (2019). Cyclic plastic deformation of rolling/sliding contact - quasistatic FE calculations using different plasticity models. *Wear* In press.

Pointner, P., Joerg, A., and Jaiswal, J. (2006). *Definitive guidelines on the use of different rail grades INNOTRACK GUIDELINE*. Tech. rep., pp. 1–45.

Qin, J., Holmedal, B., and Hopperstad, O. S. (2018). A combined isotropic, kinematic and distortional hardening model for aluminum and steels under complex strain-path changes. *International Journal of Plasticity* 101, 156–169.

Radermacher, A. and Reese, S. (2014). Model reduction in elastoplasticity: Proper orthogonal decomposition combined with adaptive sub-structuring. *Computational Mechanics* 54 (3), 677–687.

Rowan, T. (1990). "Functional Stability Analysis of Numerical Algorithms". PhD thesis. University of Texas at Austin.

Runarsson, T. P. and Yao, X. (2005). Search biases in constrained evolutionary optimization. *IEEE Transactions on Systems, Man and Cybernetics Part C: Applications and Reviews* 35 (2), 233–243.

Shi, B., Bartels, A., and Mosler, J. (2014). On the thermodynamically consistent modeling of distortional hardening: A novel generalized framework. *International Journal of Plasticity* 63, 170–182.

Skrypnyk, R. et al. (2019a). Metamodelling of wheel–rail normal contact in railway crossings with elasto-plastic material behaviour. *Engineering with Computers* 35 (1), 139–155.

Skrypnyk, R. et al. (2019b). Prediction of plastic deformation and wear in railway crossings – Comparing the performance of two rail steel grades. *Wear* 428-429, 302–314.

Sung, S.-J. et al. (2011). Evolution of yield surface in the 2D and 3D stress spaces. *International Journal of Solids and Structures* 48 (6), 1054–1069.

Tagashira, S. et al. (2000). Deformation Microstructure and Tensile Strength of Cold Rolled Pearlitic Steel Sheets. *ISIJ International* 40 (11), 1149–1156.

Terada, K. et al. (2004). Numerical re-examination of the micro-scale mechanism of the Bauschinger effect in carbon steels. *Computational Materials Science* 31 (1-2), 67–83.

Vladimirov, I. N., Pietryga, M. P., and Reese, S. (2008). On the modelling of non-linear kinematic hardening at finite strains with application to springback - Comparison of time integration algorithms. *International Journal for Numerical Methods in Engineering* 75 (1), 1–28.

Wallin, M. and Ristinmaa, M. (2005). Deformation gradient based kinematic hardening model. *International Journal of Plasticity* 21 (10), 2025–2050.

Wallin, M., Ristinmaa, M., and Ottosen, N. S. (2003). Kinematic hardening in large strain plasticity. *European Journal of Mechanics - A/Solids* 22 (3), 341–356.

Wetscher, F., Stock, R., and Pippan, R. (2007). Changes in the mechanical properties of a pearlitic steel due to large shear deformation. *Materials Science and Engineering A* 445-446, 237–243.

Wiest, M. et al. (2008). Assessment of methods for calculating contact pressure in wheel-rail/switch contact. *Wear* 265 (9), 1439–1445.

Wu, H. C. (2003). Effect of loading-path on the evolution of yield surface for anisotropic metals subjected to large pre-strain. *International Journal of Plasticity* 19 (10), 1773–1800.

You, B.-R. and Lee, S.-B. (1996). A critical review on multiaxial fatigue assessments of metals. *International Journal of Fatigue* 18 (4), 235–244.

Zhang, X. et al. (2018). Structure and strength of sub-100 nm lamellar structures in cold-drawn pearlitic steel wire. *Materials Science and Technology (United Kingdom)* 34 (7), 794–808.

Zhao, T. Z. et al. (2014). Hardening and softening mechanisms of pearlitic steel wire under torsion. *Materials and Design* 59, 397–405.